Int. J. Heat Mass Transfer. Vol. 29, No. 3, pp. 429–438, 1986
Printed in Great Britain

0017–9310/86 $3.00 + 0.00
Pergamon Press Ltd.

Effect of vapour velocity on film condensation of R-113 on horizontal tubes in a crossflow

HIROSHI HONDA,* SHIGERU NOZU,* BUNKEN UCHIMA* and TETSU FUJII†

* Department of Mechanical Engineering, Okayama University, Okayama 700, Japan
† Research Institute of Industrial Science, Kyushu University, Kasuga 816, Japan

(*Received* 24 *June* 1985 *and in final form* 23 *August* 1985)

Abstract—Film condensation of downward flowing R-113 vapour at near atmospheric pressure on single horizontal tubes was studied experimentally over wide ranges of vapour velocity and condensation temperature difference. The flow of condensate was visualized by injecting a dye tracer. Three flow regimes: smooth surface, two-dimensional waves and three-dimensional waves, were observed. In the last flow regime an abrupt thickening of the condensate film was seen at an angular position about 1.75 rad from the tube top. Turbulent mixing of condensate was observed in the thick film region. The present and earlier heat transfer results for R-113 and R-21 were compared with the laminar two-phase boundary-layer theory. The point at deviation from the theoretical prediction was found to be dependent on a dimensionless number which gave a transition criterion between smooth and wavy condensate surfaces. A correlation equation for the average heat transfer coefficient is proposed, where an equivalent Reynolds number is introduced for the high vapour velocity region.

INTRODUCTION

FORCED convection condensation on a horizontal tube has received considerable attention and an up-to-date review of literature is given by Lee and Rose [1]. Lee *et al.* [2] and Rahbar and Rose [3] compared earlier work and their own experimental results for steam, R-21, R-113 and ethylene glycol with the laminar two-phase boundary-layer theory incorporating the assumption of uniform wall temperature. The agreement between the two was generally good at low vapour velocity, while the agreement was moderate or poor, depending on the test fluid, at high vapour velocity. For steam condensation at high vapour velocity, the measured average heat transfer coefficient was lower than the theoretical prediction, with the difference increasing with the vapour velocity. For R-113 condensation at moderate-to-high vapour velocity, on the other hand, the measured value was higher than the theoretical prediction and depended strongly on the tube diameter. The ethylene glycol results showed an intermediate character between the steam and R-113 results.

Previous theoretical studies [4–8] have shown that the steam results can be predicted reasonably well by a vapour-to-coolant heat transfer theory which takes account of wall temperature variation around the tube. However, this theory fails to predict the R-113 results. Recently, Rose [9] proposed a theory taking account of pressure variation around the tube in the momentum equation for the condensate film, which has been neglected in many of the previous studies. However, this theory still predicts a lower value of the average heat transfer coefficient for R-113 condensation at high vapour velocity, and fails to predict the dependence on the tube diameter.

The present work was undertaken to obtain a better understanding of refrigerant condensation at high vapour velocity using R-113 as a test fluid.

TEST APPARATUS AND PROCEDURE

The test apparatus, shown schematically in Fig. 1, consists of a closed natural circulation loop of test fluid and a closed, forced-circulation loop of coolant. The test fluid loop is made of stainless steel except for a test section which is made of brass. The R-113 vapour generated in an electrically heated boiler (1) with a maximum output of 45 kW flows through electric superheaters (2) and a calming section (3), fitted with a honeycomb and two 200-mesh screens, into the test

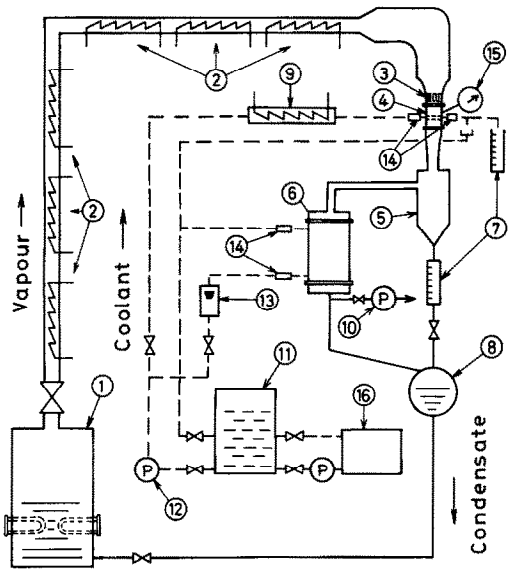

FIG. 1. Schematic diagram of test apparatus: (1) boiler, (2) superheater, (3) calming section, (4) test section, (5) drain separator, (6) dump condenser, (7) measuring glass tube, (8) condensate receiver, (9) heater, (10) vacuum pump, (11) coolant tank, (12) feed pump, (13) rotameter, (14) mixing chamber, (15) pressure gauge, (16) chilling unit.

NOMENCLATURE

A	dimensionless number, Pr_l/FrH
B	dimensionless number, Pr_l/RH
c_p	specific heat at constant pressure
d	tube diameter
Fr	Froude number, u_∞/gd
H	phase-change number, $c_{pl}\Delta T/h_{fg}$
h	width of vapour passage normal to tube
h_{fg}	specific enthalpy of evaporation
K	dimensionless number, $FrRe_fNu/(1-\rho_v/\rho_l)$
l	condensing length of tube
Nu	average Nusselt number, $\alpha d/\lambda_l$
Pr	Prandtl number
Q	heat transfer rate to coolant
Q_l	heat loss to environment
q	average heat flux
R	$\rho\mu$ ratio, $(\rho_l\mu_l/\rho_v\mu_v)^{1/2}$
Re_{eq}	equivalent Reynolds number, $[Re_f + Re_L(\rho_v/\rho_l)^{1/2}]$
Re_f	film Reynolds number, $2\pi dq/\mu_l h_{fg}$
Re_L	two-phase Reynolds number, $u_\infty d/v_l$
T_c	average coolant temperature
T_s	saturation temperature
T_w	local wall temperature
T_{wm}	average wall temperature
T_{wz}	circumferential average wall temperature
ΔT	average condensation temperature difference, $(T_s - T_{wm})$
u_∞	oncoming velocity of vapour
X	dimensionless number, $(1+B)^{2/3}/A^{1/2}$
z	axial distance measured from coolant inlet.

Greek symbols

α	average heat transfer coefficient
α_z	circumferential average heat transfer coefficient
λ	thermal conductivity
μ	dynamic viscosity
ν	kinematic viscosity
ρ	density
ϕ	angle at abrupt change of condensate film thickness.

Subscripts

c	calculated value by equation (11)
l	condensate; also calculated value by equation (5)
t	calculated value by equation (10)
v	vapour.

section (4). A small part of the vapour condenses on a test tube. The remaining vapour and condensate flow into a drain separator (5) and the separated vapour completely condenses in a dump condenser (6). The condensate returns to the boiler through a condensate receiver (8). The air-tightness of the loop was such that the pressure rise under vacuum condition was less than 50 Pa h^{-1}. The loop was thermally insulated by fibre glass. The coolant is pumped from a coolant tank (11) to the test tube through an electric heater (9), and also to the dump condenser through a rotameter (13). Mixing chambers (14) are installed at the inlets and exits of the test tube and the dump condenser. The coolant temperature in the coolant tank is regulated by a chilling unit (16).

The test section is a vertical rectangular ducting with internal dimensions of 110 × 100 mm. The test tube is positioned horizontally across the smaller dimension of the duct. Each duct wall parallel to the tube is fitted with a viewing window. In the test of higher vapour velocity, the width of the vapour passage normal to the test tube is reduced by attaching a pair of removable plates made of glass and polyvinyl chloride (PVC).

Two copper tubes of 8.0 mm O.D. × 5.0 mm I.D. and 19.0 mm O.D. × 16.0 mm I.D. were tested. Figure 2 shows the 19-mm-O.D. tube fitted to the test section. The tube was made up of five short tubes. Adjoining ends of the short tubes were machined over a 5 mm length as shown in Fig. 2. Three or four grooves of about 0.5 × 0.5 mm were cut axially $\pi/2$ rad apart on the inner contacting surfaces, and Teflon-insulated, 0.127-mm-diam. constantan wires with bare tips were embedded in the grooves. Thus 15 thermocouples were arranged between the constantan wires and the tube itself, where the contacting surfaces were soldered to form a tube. The wires were led out through the coolant passage. The test tube was positioned so that the thermocouples' hot junctions were located at the top, sides and bottom of the tube. To increase the coolant velocity, a PVC rod of 10 mm in diameter was inserted concentrically in the tube. The 8-mm-O.D. tube was similarly fitted with 11 wall thermocouples in the centre cross-section and in the cross-sections 10 mm apart from the side walls.

The coolant temperatures in the inlet and exit mixing chambers of the test tube were measured by five-junction copper–constantan thermopiles. The coolant temperatures in the inlet and exit mixing chambers of the dump condenser, the vapour temperatures 100 mm upstream and downstream of the test tube, and the condensate temperature just before returning to the boiler were measured by chromel–alumel sheathed thermocouples. Readings of the thermocouple and thermopile e.m.f.s were periodically repeated six times by using a data acquisition system equipped with a digital voltometer of 1 μV resolution. The vapour pressure in the test section was measured by a precision Bourdon tube gauge, reading to 10^3 Pa, connected to a pressure tap on the side wall, 100 mm upstream of the

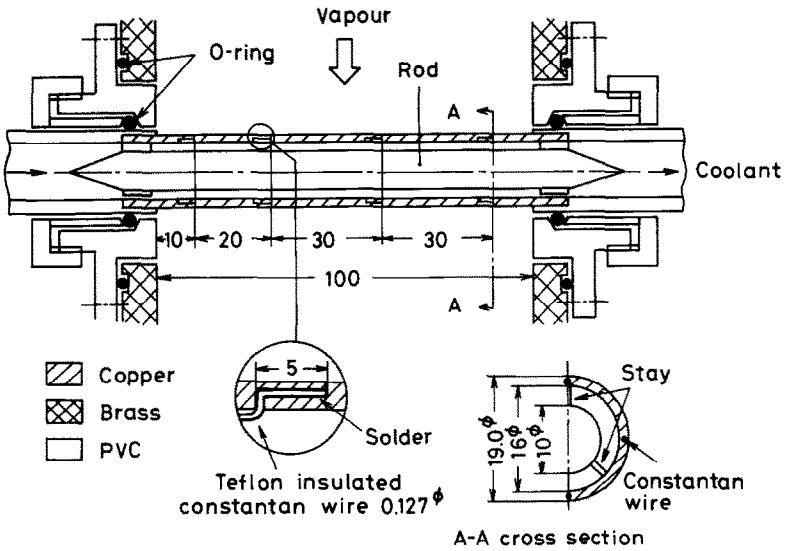

FIG. 2. Details of 19-mm-O.D. tube attached to test section.

test tube. The coolant flow rate in the test tube and condensation rate on the test tube were measured by measuring glass tubes [(7) in Fig. 1] and a stop watch. All the measured data were processed by the data acquisition system.

Condensate flow on the 19-mm-O.D. tube was visualized by injecting the R-113 solution of a blue dye as a tracer. For the injection of the tracer, a fine stainless-steel tube of 0.5 mm O.D. was inserted into the test section, and the tip of the tube was brought in contact with the top of the test tube near the central cross section. Still photographs were taken by a 35-mm camera at about 1 m horizontal distance from the test tube.

Experiments were conducted at a vapour pressure slightly above atmospheric pressure (about 0.12 MPa). To avoid condensation on the wall of the vapour supply duct, the vapour was superheated by several degrees.

Table 1 shows the ranges of experimental conditions, where d denotes the tube outer diameter, h the width of vapour passage normal to the tube, T_s the saturation temperature, T_{wm} the area average wall temperature, $\Delta T = T_s - T_{wm}$ the average condensation temperature difference, and u_∞ the vapour incoming velocity. T_s was obtained from the measured vapour pressure; the value of T_s agreed with the readings of the sheathed thermocouples inserted in the test section to within ± 0.1 K when the superheaters were switched off. T_{wm} was calculated from the local wall temperatures, which were slightly corrected for the radial wall conduction. u_∞ was calculated from the mass flow rate of R-113 by using the thermodynamic state in the test section. The mass flow rate was obtained from the electric power supply to the boiler by applying a thermal energy balance between the boiler inlet and exit. Heat loss from the boiler was estimated by using a calibration curve obtained by preliminary experiments in which the condensate flow rate returning to the boiler was also measured by a gear flow meter. The heat loss was less than 5% of the electric power supply.

Table 1. Ranges of experimental conditions

d (mm)	h (mm)	d/h	T_s (°C)	T_{wm} (K)	ΔT (K)	u_∞ (m s^{-1})
8.0	23	0.348				
	32	0.250	53–54	21–51	3–32	0.36–15.6
	110	0.073				
19.0	45	0.422	48–52	22–51	3–29	0.34–8.5
	110	0.173				

The average heat transfer coefficient α and the average Nusselt number Nu are defined as

$$\alpha = (Q + Q_l)/\pi d l \Delta T = q/\Delta T, \quad Nu = \alpha d/\lambda_l \qquad (1)$$

where Q is the heat transfer rate calculated from the flow rate and temperature rise of the coolant, Q_l is the heat loss to the environment, l is the condensing length of the test tube (= 100 mm) and q is the average heat flux. For each tube a calibration curve for Q_l was obtained by preliminary experiments in which the test tube was thermally insulated by a PVC block. The value of Q_l was less than 13% of Q. The accuracy of the measured α value is estimated to be within 7%. In the data reduction the physical properties of condensate were evaluated at the reference temperature $T_r = T_{wm} + 0.3(T_s - T_{wm})$.

RESULTS AND DISCUSSION

Wall temperature distribution

The measured values of local wall temperature varied in both axial and circumferential directions. Figure 3 shows the examples of wall temperature distribution for the 19-mm-O.D. tube, which exhibited

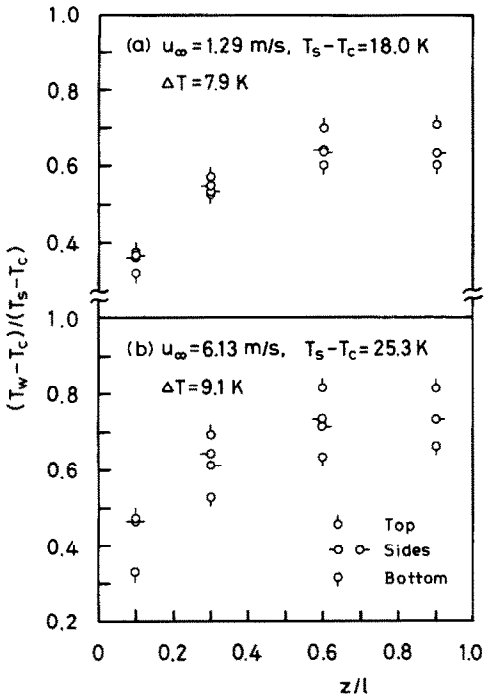

FIG. 3. Axial wall temperature distribution along 19-mm-O.D. tube.

greater variations as compared to the 8-mm-O.D. tube. The ordinate is the dimensionless wall temperature $(T_w-T_c)/(T_s-T_c)$ and the abscissa is the dimensionless length measured from the coolant inlet z/l. It is seen that both axial and circumferential variations of the dimensionless condensation temperature difference $1-(T_w-T_c)/(T_s-T_c)$ are greater for higher u_∞.

It is relevant to discuss the effect of wall temperature variation on the average heat transfer coefficient. The dependence of the circumferential average heat transfer coefficient α_z on the circumferential average condensation temperature difference ΔT_z may be assumed as

$$\alpha_z = a\Delta T_z^{-n} \tag{2}$$

where a is the proportionality constant. The average heat transfer results as shown later in Fig. 5 suggests $n \lesssim 1/4$. Then, α can be obtained by

$$\alpha = \int_0^1 \alpha_z \Delta T_z \, dz/l\Delta T = a\int_0^1 \Delta T_z^{1-n} \, dz/l\Delta T \tag{3}$$

where

$$\Delta T = \int_0^1 \Delta T_z \, dz/l.$$

Alternatively, substitution of ΔT into ΔT_z in equation (2) yields

$$\alpha = \Delta T^{-n}. \tag{4}$$

Comparison of α values given by equations (3) and (4), which were calculated by using a smooth curve fit for ΔT_z and $n = 1/4$, revealed that the difference between the two was less than 1%. Thus, the wall temperature with axial variation can be represented by the axially averaged value.

Previous theoretical studies [4–8] have shown that the circumferential wall temperature variation causes a decrease in α value as compared to the case of uniform wall temperature. Comparisons were made between the uniform and variable wall temperature solutions obtained for the present experimental condition by using the computer program described in ref. [8]. The difference in α values increased as u_∞ increased and reached 7% at the highest u_∞. It should be mentioned here that, while the theory assumed a laminar condensate film, the observed condensate flow at moderate to high vapour velocity was not laminar (see Fig. 4). However, since the observed circumferential wall temperature variation was smaller than the prediction of the variable wall temperature theory, it is probable that the deviation of the measured α value from that to be obtained for the uniform wall temperature condition is less than 7%.

Flow pattern

Figures 4(a)–(e) compare typical photographs showing the condensate film on the 19-mm-O.D. tube at different values of u_∞. The average heat transfer data corresponding to these photographs are shown by a symbol ☆ in Figs. 5–9. The tube surface was slightly roughened with No. 1000 emery paper to get a diffuse light reflection. The flow rate of the tracer was held at about 3.5×10^{-3} g s^{-1}. The streak width on the upper half of the tube is from 2.2 to 3.0 mm. Thus the flow rate of the tracer per unit streak width is from 4.3 to 5.9 kg m^{-1} h^{-1}. This value is 20–32% of the condensate flow rate per unit tube length at the bottom on one side of the tube.

At very low u_∞ a laminar condensate film with smooth circumferential flow of the tracer is observed [Fig. 4(a)]. With a slight increase in u_∞ two-dimensional waves appear on the condensate surface as seen from lights and shades on the tracer [Fig. 4(b)]. In Fig. 4(c) three-dimensional waves (characterized by a pebbled appearance) having a wavelength of about 1.5 mm are observed on the upper half of the tube. It is also seen that the streak bends at an angle $\phi \simeq 1.75$ rad from the tube top and the condensate film thickness changes more or less abruptly at this point. These results suggest the presence of recirculating vapour flows in the separated region of the vapour boundary layer. With a further increase in u_∞ the wavelength on the upper half of the tube becomes smaller, and the condensate film thickness changes more sharply at the point at $\phi \simeq 1.75$ rad [Fig. 4(d)]. The boundary of the thin and thick film regions is irregular, and small droplets of condensate are entrained from the vicinity of the boundary into the vapour flow. These results suggest the instability in the condensate film as described by Rose [9]. At the highest value of u_∞ shown in Fig. 4(e) the film surface on the upper half of the tube has a very fine roughness. A

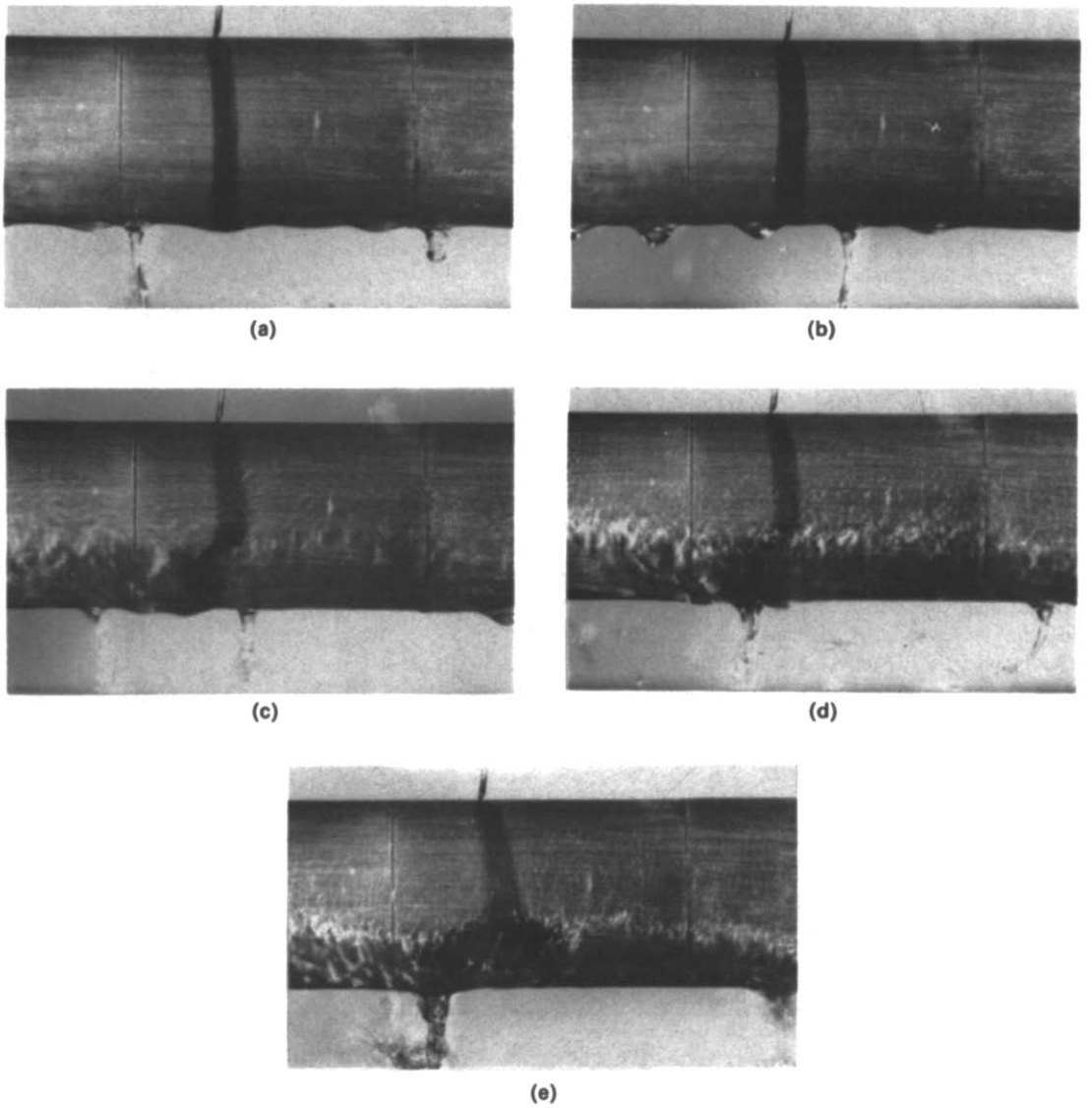

FIG. 4. Typical photographs of condensate film on 19-mm-O.D. tube: $h = 45$ mm and $\Delta T \simeq 10$ K. (a) $u_\infty = 1.5\,\mathrm{m\,s^{-1}}$, $q = 18.3\,\mathrm{kW\,m^{-2}}$. (b) $u_\infty = 1.8\,\mathrm{m\,s^{-1}}$, $q = 17.0\,\mathrm{kW\,m^{-2}}$. (c) $u_\infty = 3.3\,\mathrm{m\,s^{-1}}$, $q = 21.3\,\mathrm{kW\,m^{-2}}$. (d) $u_\infty = 5.5\,\mathrm{m\,s^{-1}}$, $q = 29.1\,\mathrm{kW\,m^{-2}}$. (e) $u_\infty = 8.4\,\mathrm{m\,s^{-1}}$, $q = 38.7\,\mathrm{kW\,m^{-2}}$.

considerable broadening and a rather indistinct boundary of the tracer on the lower half indicate turbulent mixing. The condensate leaving the tube bottom forms agglomerations as described by Lee *et al.* [2]. No marked variation of the condensate film behaviour along the tube axis is observed in every figure, though there were considerable axial variations of tube wall temperature as shown in Fig. 3. The observed behaviour of the condensate film on the upper half of the tube is qualitatively in accord with the transition of horizontal stratified gas–liquid flow described by Hanratty and Engen [10]. In the present results, however, the wavelength was much smaller and roll waves were not observed, probably as a result of very thin film thickness.

Table 2 compares the measured values of the angle at abrupt change of condensate film thickness and the average Nusselt number for cases (c)–(e) in Fig. 4 with those theoretically predicted by Honda and Fujii [8] and Rose [9]. The measured value of ϕ was defined as the point where bending or broadening of the tracer was observed. In Honda and Fujii's analysis, ϕ was defined as the separation point of the vapour boundary layer, which depends on the assumed mainstream velocity distribution around the tube. The solutions for the potential flow and the flow corresponding to the measured static pressure distribution of Roshko [11] are presented in Table 2 with subscripts P and R, respectively. In the Rose's analysis, which assumed the potential flow, ϕ was defined as the point where the

Table 2. Comparison of measured values with theoretical predictions* for angle at abrupt change of condensate film thickness and average Nusselt number

Case	u_∞ (m s^{-1})	ϕ (rad)	ϕ_R (rad)	ϕ_P (rad)	ϕ_{PR} (rad)	Nu	Nu_R	Nu_P	Nu_{PR}
(c)	3.27	1.75	1.58	2.04	2.06	537	443	500	481
(d)	5.45	1.75	1.57	2.03	1.76	791	494	581	578
(e)	8.41	1.8	1.58	2.04	1.71	1013	547	666	671

* Subscripts R and P refer to Honda and Fujii theory [8] for the Roshko's flow and the potential flow, respectively, and subscript PR to Rose theory [9] for the potential flow.

circumferential increment rate of the condensate film thickness becomes infinite as a result of positive pressure gradient in the condensate film. This solution is denoted with a subscript PR. It is seen that the measured values of ϕ lie in between ϕ_R and ϕ_P, and agree well with ϕ_{PR} for cases (d) and (e) though the dependence of ϕ_{PR} on u_∞ is not in accord with that of ϕ. On the other hand, the measured values of Nu are greater than the theoretical predictions and the difference increases as u_∞ increases. This enhancement in heat transfer is expected from the surface waves and the turbulent mixing in the condensate film observed in Figs. 4(c)–(e).

Average heat transfer

Figure 5 shows the average heat transfer results for three sets of d and h plotted on the coordinates of $Nu/\sqrt{Re_L}$ vs $A = Pr_l/FrH$ with u_∞ as a parameter, where $Re_L = u_\infty d/\nu_l$ is the two-phase Reynolds number, $Fr = u_\infty^2/gd$ is the Froude number and $H = c_{pl}\Delta T/h_{fg}$ is the phase-change number. The solid and dotted lines show the following expressions, which are derived from numerical analyses with the assumption of laminar film and uniform wall temperature

$$Nu/\sqrt{Re_L} = 0.728A^{1/4}(1+X+0.57X^2)^{1/4} \quad (5)$$

$$Nu/\sqrt{Re_L} = 0.725A^{1/4}(1+2.38X^2)^{1/4} \quad (6)$$

where $X = (1+B)^{2/3}/A^{1/2}$, $B = Pr_l/RH$ and $R = (\rho_v\mu_v/\rho_l\mu_l)^{1/2}$. While equation (5) is based on the assumption of the Roshko's flow [11] for the mainstream velocity distribution around the tube [7], equation (6) is based on the assumption of the potential flow [12]. For each equation, two lines corresponding to the smallest and the largest values of ΔT in the present experimental data are presented. Nusselt's equation [13] is also shown by chain lines for reference. It should be mentioned in comparison between the measured values and the theoretical expressions that ΔTdecreases with increase in A for the same u_∞ value in

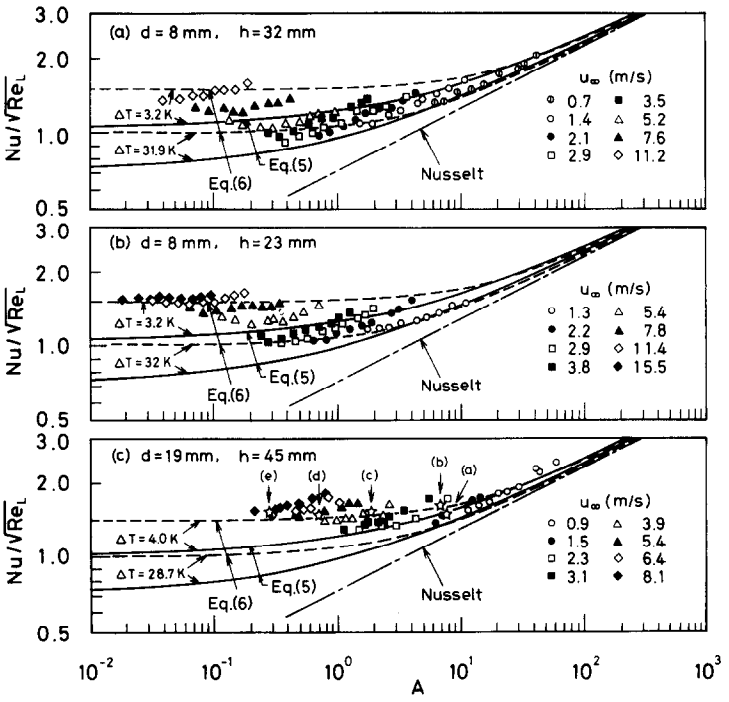

FIG. 5. Experimental data plotted on the coordinates of $Nu/\sqrt{Re_L}$ vs A.

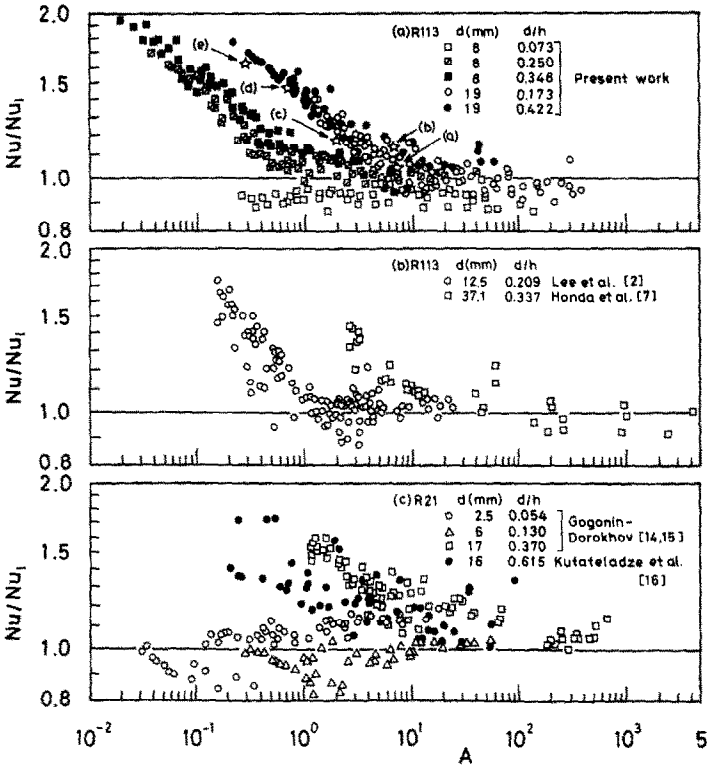

FIG. 6. Comparison of present and earlier experimental data for R-113 and R-21 with equation (5).

the experimental data, while isothermal lines are presented for the theoretical results. The agreement between theory and experiment is fairly good for high A value, i.e. for low u_∞ value in magnitude and tendency. However, the experimental data show a stronger rate of increase of $Nu/\sqrt{Re_L}$ with u_∞ than indicated by theory at high u_∞. This tendency is in accord with previous studies [2, 3, 7]. It is also seen from comparison of Figs. 5(a) and (b) that the $Nu/\sqrt{Re_L}$ value at constant u_∞ is higher for smaller h. This indicates the effect of tunnel blockage which acts to modify the mainstream velocity distribution around the tube.

Figure 6 shows the ratio of the measured Nu value to Nu_1 calculated from equation (5). In the figure the R-113 results of Lee *et al.* [2] and Honda *et al.* [7], and the R-21 results of Gogonin and Dorokhov [14, 15] and Kutateladze *et al.* [16] are also included. Since the experiments by Kutateladze *et al.* are concerned with a tube bundle, only the results for the first row are quoted. The experimental data in Fig. 6 are separated into two regions in tendency, i.e. those for the larger and smaller values of A. In the former region $Nu/Nu_1 \simeq 1$, and in the latter region the Nu/Nu_1 value increases with decrease in A except for the R-21 data for the 2.5- and 6-mm-O.D. tubes. The value of A at the boundary between the two regions becomes larger as d increases. In the above-mentioned tendency a weak dependence on the blockage ratio h/d is also seen as in Fig. 6(a). The experimental data denoted by the symbol ☆ and (a)–(e) correspond to the photographs in Fig. 4. It is clear that the increase in the Nu/Nu_1 value at smaller A is related to the change of flow pattern of the condensate film.

Taitel and Dukler [17] presented the transition criterion between the stratified smooth and stratified wavy regimes for the horizontal gas–liquid flow as

$$K = \rho_1\rho_v u_\infty^2 u_l/(\rho_1-\rho_v)\mu_l g \simeq 400. \quad (7)$$

If this criterion can be applied to the present case, the dimensionless number K may be rewritten as

$$K = \frac{\rho_v u_\infty^2}{(\rho_1-\rho_v)gd}\frac{\rho_1 u_l \delta}{\mu_l}\frac{d}{\delta} = \frac{\rho_v}{(\rho_1-\rho_v)} FrRe_f Nu \quad (8)$$

where δ is the average condensate film thickness and u_l is the average velocity of condensate.

The same data as in Fig. 6 are plotted on the coordinates of Nu/Nu_1 vs K in Fig. 7. It is seen that the values of K at deviation from $Nu/Nu_1 = 1$ are about the same magnitude among the data set, i.e. $K \simeq 1000$ except for the R-21 results for the 2.5- and 6-mm-O.D. tubes. It should be mentioned here that marked systematic deviation from $Nu/Nu_1 = 1$ is not seen in the ethylene glycol results of Rahbar and Rose [3], because their data are limited in the range $10^{-1} \lesssim K \lesssim 3\times10^3$.

To correlate the experimental data in the higher u_∞ region, the equivalent Reynolds number is introduced as

$$Re_{eq} = Re_f + Re_L(\rho_v/\rho_l)^{1/2} \quad (9)$$

where $Re_f = 2\pi dq/\mu_l h_{fg}$ is the film Reynolds number. Figure 8 shows the experimental data plotted on the

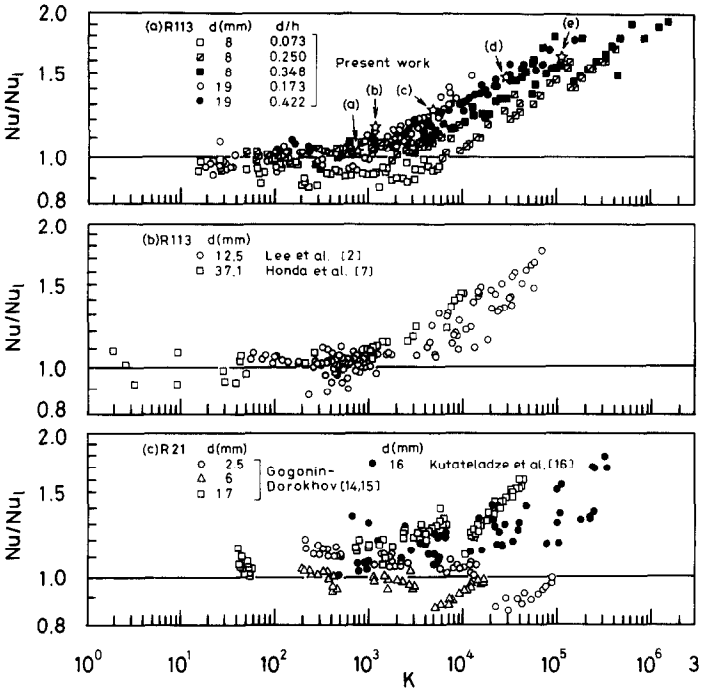

FIG. 7. Present and earlier experimental data for R-113 and R-21 plotted on the coordinates of Nu/Nu_l vs K.

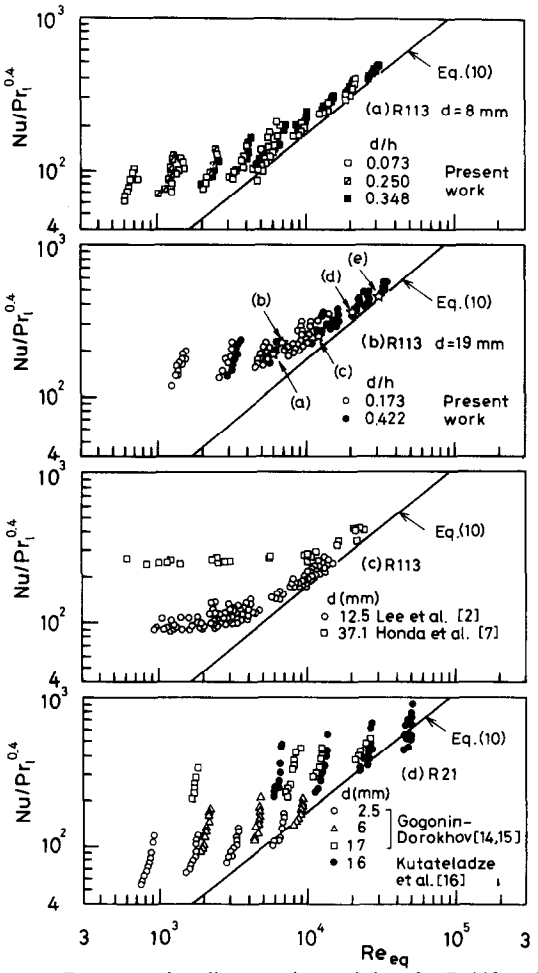

FIG. 8. Present and earlier experimental data for R-113 and R-21 plotted on the coordinates of $Nu/Pr_l^{0.4}$ vs Re_{eq}.

coordinates of $Nu/Pr_l^{0.4}$ vs Re_{eq}, where the index of Pr_l has been determined after some trials. The solid line in the figure represents the following expression

$$Nu_t = 0.11\, Re_{eq}^{0.8} Pr_l^{0.4}. \quad (10)$$

It is seen that the R-113 data shown in Figs. 8(a)–(c) asymptotically approach the solid line with the increase in Re_{eq}. The same trend is observed for the R-21 data shown in Fig. 8(d) though a part of the data is lower than the solid line at large Re_{eq}.

For an intermediate value of u_∞ where both equations (5) and (10) give lower predictions, the following expression provides a good fit to the experimental data

$$Nu_c = (Nu_l^4 + Nu_t^4)^{1/4}. \quad (11)$$

Figure 9 shows the ratio Nu/Nu_c plotted as a function of A. For the R-113 data shown in Figs. 9(a) and (b), the deviation of the measured values from equation (11) is within $\pm 15\%$ except for a part of the data at $d = 8$ mm and $d/h = 0.073$ at higher u_∞. For the R-21 data shown in Fig. 9(c) the deviation is within about $\pm 20\%$.

CONCLUSIONS

Experiments were made in wide ranges of vapour velocity and condensation temperature difference using R-113 as a test fluid. Condensate flow was visualized by using a dye tracer. The conclusions are as follows:

(1) The surface of the condensate film on the upper half of the tube undergoes transitions of smooth surface, two- and three-dimensional waves, with the

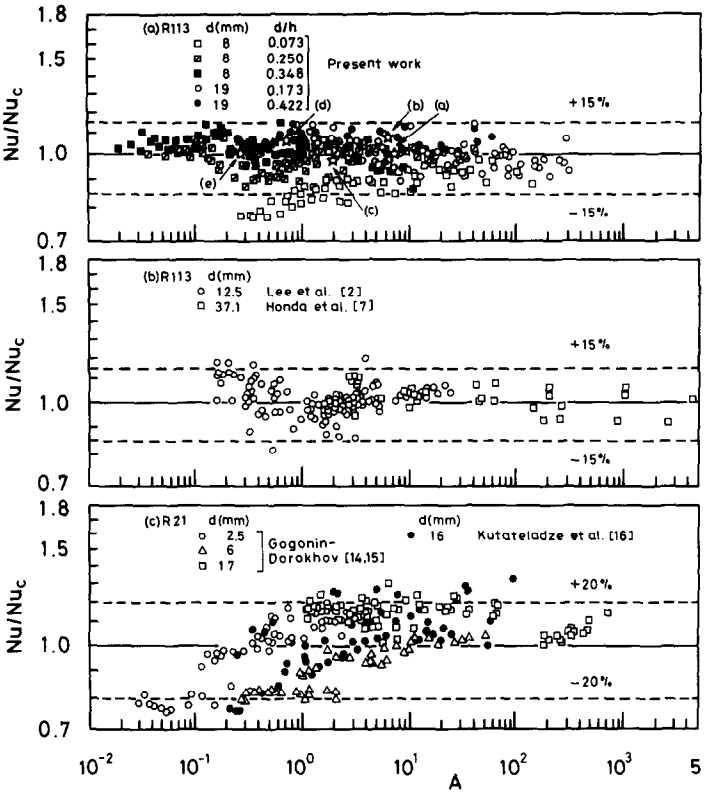

FIG. 9. Comparison of present and earlier experimental data for R-113 and R-21 with equation (11).

wavelength decreasing with increase in vapour velocity.

(2) In the three-dimensional wave regime, the thickness of the condensate film changes abruptly at an angular position about 1.75 rad from the tube top. The boundary of the thin and thick film regions is irregular and small droplets of condensate are entrained from the vicinity of the boundary into the vapour flow. Turbulent mixing occurs in the thick film region at high vapour velocity.

(3) Heat transfer characteristics are closely connected with the condensate flow pattern on the tube. The point at deviation of the measured average heat transfer coefficient from the prediction of the laminar two-phase boundary-layer theory is given by the transition criterion between the smooth and wavy condensate surfaces as $K \simeq 1000$.

(4) The present and earlier experimental data for R-113 and R-21 in the high vapour velocity region can be correlated by using the concept of the equivalent Reynolds number. The correlation is given by equation (10).

(5) Most of the experimental data for the whole range of vapour velocity are correlated well by equation (11).

Acknowledgements—This work was partly supported by the Ministry of Education, Science and Culture through a Grant in Aid for Scientific Research, Project No. 58550153.

REFERENCES

1. W. C. Lee and J. W. Rose, Film condensation on a horizontal tube—effect of vapour velocity, *Proc. 7th Int. Heat Transfer Conference*, Munich, Vol. 5, pp. 101–106 (1982).
2. W. C. Lee, S. Rahbar and J. W. Rose, Film condensation of refrigerant-113 and ethanediol on a horizontal tube—effect of vapor velocity, *J. Heat Transfer* **106**, 524–530 (1984).
3. S. Rahbar and J. W. Rose, New measurements for forced-convection film condensation, *Proc. 1st U.K. Heat Transfer Conference, Inst. Chem. Engrs. Symp. Ser.* No. 76, pp. 619–632 (1984).
4. A. A. Nicol and D. J. Wallace, Condensation with appreciable vapour velocity and variable wall temperature, *Proc. Symposium on Steam Turbine Condensers*, NEL Report No. 619, pp. 27–38 (1976).
5. A. A. Nicol, A. Bryce and A. S. A. Ahmed, Condensation of a horizontally flowing vapour on a horizontal cylinder normal to the vapour stream, *Proc. 6th Int. Heat Transfer Conference*, Toronto, Vol. 2, pp. 401–406 (1978).
6. D. W. Nobbs and Y. R. Mayhew, Effect of downward vapour velocity and inundation on condensation rates on horizontal tube banks, *Proc. Symposium on Steam Turbine Condensers*, NEL Report No. 619, pp. 39–52 (1976).
7. H. Honda, S. Nozu and T. Fujii, Vapour to coolant heat transfer during condensation of flowing vapour on a horizontal tube, *Proc. 7th Int. Heat Transfer Conference*, Munich, Vol. 5, pp. 157–161 (1982).
8. H. Honda and T. Fujii, Condensation of flowing vapor on a horizontal tube—numerical analysis as a conjugate heat transfer problem, *J. Heat Transfer* **106**, 841–848 (1984).
9. J. W. Rose, Effect of pressure gradient in forced convection

condensation on a horizontal tube, *Int. J. Heat Mass Transfer* **27**, 39–47 (1984).
10. T. J. Hanratty and J. M. Engen, Interaction between a turbulent air stream and a moving water surface, *A.I.Ch.E. Jl* **3**, 299–304 (1957).
11. A. Roshko, A new hodograph for free-streamline theory, NACA TN3168 (1954).
12. T. Fujii, H. Uehara and C. Kurata, Laminar film-wise condensation of flowing vapour on a horizontal cylinder, *Int. J. Heat Mass Transfer* **15**, 235–246 (1972).
13. W. Nusselt, Die Oberflächenkondensation des Wasserdampfes, *Z. Ver. dt. Ing.* **60**, 541–546, 569–575 (1916).
14. I. I. Gogonin and A. R. Dorokhov, Heat transfer from condensing Freon-21 vapour moving over a horizontal tube, *Heat Transfer—Sov. Res.* **3**, 157–161 (1971).
15. I. I. Gogonin and A. R. Dorokhov, Experimental investigation of heat transfer with condensation of moving vapour of Freon-21 on horizontal cylinders, *J. appl. Mech. tech. Phys.* **17**, 252–257 (1976).
16. S. S. Kutateladze, I. I. Gogonin, A. R. Dorokhov and V. I. Sosunov, Film condensation of flowing vapour on a bundle of plain horizontal tubes, *Thermal Engng* **26**, 270–273 (1979).
17. Y. Taitel and A. E. Dukler, A method for predicting flow regime transition in horizontal and near horizontal gas–liquid flow, *A.I.Ch.E. Jl* **22**, 47–55 (1976).

EFFET DE LA VITESSE DE LA VAPEUR SUR LA CONDENSATION EN FILM DE R113 SUR DES TUBES HORIZONTAUX EN ECOULEMENT TRANSVERSAL

Résumé—La condensation en film d'une vapeur descendante de R113, à la pression atmosphérique, sur un tube unique horizontal est étudiée expérimentalement pour un large domaine de vitesse de vapeur et de différence de température. Le débit de condensat est visualisé par injection d'un traceur. On observe trois régimes d'écoulement: surface lisse, rides bidimensionnelles et rides tridimensionnelles. Dans le dernier régime, un brusque épaississement du film liquide est constaté à une position angulaire d'environ 1,75 rad à partir du sommet du tube. On observe un mélange turbulent de condensat dans la région épaisse du film. Les résultats thermiques présents et antérieurs pour R113 et R21 sont comparés avec la théorie de la couche limite laminaire diphasique. Le point où il y a déviation dépend d'un nombre adimensionnel qui fournit un critère de transition entre des surfaces lisses ou ridées de condensat. Une formule pour le coefficient moyen de transfert thermique est proposée dans laquelle un nombre de Reynolds équivalent est introduit pour la région de grande vitesse de vapeur.

EINFLUSS DER DAMPFGESCHWINDIGKEIT AUF DIE FILMKONDENSATION VON R113 AN HORIZONTALEN ROHREN IM KREUZSTROM

Zusammenfassung—Die Filmkondensation von abwärts strömendem R113-Dampf nahe Atmosphärendruck an einzelnen horizontalen Rohren wurde experimentell über weite Bereiche von Dampfgeschwindigkeit und Kondensationstemperaturdifferenzen studiert. Die Kondensatströmung wurde durch Farbspurinjektion sichtbar gemacht. Drei Strömungsregime wurden beobachtet: glatte Oberfläche, zwei- und dreidimensionale Wellen. Beim letztgenannten Strömungsregime wurde eine abrupte Verdickung des Kondensatfilms bei einem Winkel von etwa 100 grad von der Rohroberkante beobachtet. Turbulente Kondensatvermischung wurde in der Region mit dickem Film beobachtet. Die aktuellen und früheren Meßergebnisse für R113 und R21 wurden mit der laminaren Zweiphasen-Grenzschichttheorie verglichen. Der Punkt der Abweichung von der theoretischen Berechnung hängt von einer dimensionslosen Kennzahl ab, die Kriterium für den Umschlag zwischen glatter und welliger Kondensatoberfläche angibt. Eine Korrelationsgleichung für mittlere Wärmeübergangskoeffizienten wird vorgeschlagen, wobei eine äquivalente *Re*-Zahl für das Gebiet mit hoher Dampfgeschwindigkeit eingeführt wird.

ВЛИЯНИЕ СКОРОСТИ ДВИЖЕНИЯ ПАРА R-113 НА ПЛЕНОЧНУЮ КОНДЕНСАЦИЮ НА ГОРИЗОНТАЛЬНЫХ ТРУБАХ ПРИ ПОПЕРЕЧНОМ ИХ ОБТЕКАНИИ

Аннотация—Экспериментально исследуется пленочная конденсация нисходящего потока пара R-113 при давлении, близком к атмосферному, на одиночных горизонтальных трубах в широком диапазоне изменения скорости движения пара. Течение конденсата визуализировалось вдуваемым красящим индикатором. Рассматривались три режима течения жидкой пленки: невозмущенная поверхность, двумерные и трехмерные волны на поверхности пленки. В последнем режиме наблюдалось резкое утончение пленки конденсата для кольцевого слоя на расстоянии около 1,75 радиуса торца трубы. Турбулентное перемешивание конденсата наблюдалось в области толстой пленки. Результаты, полученные в настоящей работе и ранее для R-113 и R-21, сравнивались с теоретическими для ламинарного двухфазного пограничного слоя. Найдено, что величина отклонения зависит от безразмерного параметра, который является критерием переноса в области между режимами течения для гладкой и волнистой поверхностей конденсата. Предложено коррелирующее уравнение для осредненного коэффициента переноса, в которое введено эквивалентное число Рейнольдса для высоких скоростей пара.